

1 **A field study on ice melting and breakup in a boreal lake, Pääjärvi,
2 in Finland**

3 Yaodan Zhang^{1,2}, Marta Fregona³, John Loehr², Joonatan Ala-Könni⁴, Shuang Song^{5,6}, Matti
4 Leppäranta⁴, and Zhijun Li¹

5 ¹State Key Laboratory of Coastal and Offshore Engineering, Dalian University of Technology, Dalian, China

6 ²Lammi Biological Station, University of Helsinki, Finland

7 ³Department of Civil, Environmental and Mechanical Engineering, University of Trento, Trento, Italy

8 ⁴Institute of Atmospheric and Earth Sciences, University of Helsinki, Helsinki, Finland

9 ⁵Water Conservancy and Civil Engineering College, Inner-Mongolia Agricultural University, Hohhot, China

10 ⁶College of Water Conservancy, Shenyang Agricultural University, Shenyang, China

11 *Correspondence to:* Zhijun Li (lizhijun@dlut.edu.cn), Yaodan Zhang (zhangyaodan@mail.dlut.edu.cn).

12 **Abstract.** Lake ice melting and breakup form a fast, nonlinear process with important mechanical,
13 chemical, and biological consequences. The process is difficult to study in the field due to safety issues,
14 and therefore only little is known about its details. In the present work, the field data were collected on
15 foot, by hydrocopter, and by boat for a full time-series of the evolution of ice thickness, structure, and
16 geochemistry through the melting period. The observations were made in Lake Pääjärvi in 2018 (pilot
17 study) and 2022. In 2022, the maximum thickness of ice was 55 cm with 60 % snow-ice, and in 40 days
18 the ice melted by 33 cm from the surface and 22 cm from the bottom while the porosity increased from
19 less than 5% to 40–50 % at breakup. In 2018, the snow-ice layer was thin, and bottom and internal
20 melting dominated the ice decay. The mean melting rates were 1.31 cm d^{-1} in 2022 and 1.55 cm d^{-1} in
21 2018. In 2022 the electrical conductivity (EC) of ice was $11.4 \pm 5.79 \mu\text{S cm}^{-1}$, one order of magnitude
22 lower than in the lake water, and ice pH was 6.44 ± 0.28 , lower by 0.4 than in water. The pH and EC
23 of ice and water decreased along the ice decay except for slight increases in ice due to flushing by lake
24 water. Chlorophyll *a* was less than $0.5 \mu\text{g L}^{-1}$ in porous ice, approximately one-third of that in the lake
25 water. The results are important for understanding the process of ice decay with consequences to lake
26 ecology, further development of numerical lake ice models, and modeling the safety of ice cover and ice
27 loads.

28 **1 Introduction**

29 Lake ice is a thin layer between the atmosphere and lake water body and plays an important role in the
30 local environment and human life (Leppäranta, 2015). Lake ice affects the local weather by altering the
31 heat, mass and momentum exchange between the atmosphere and lake water body, as seen in the
32 surface roughness, surface temperature and albedo (Ellis and Johnson, 2004; Rouse et al., 2008a, 2008b;
33 Williams et al., 2004). The physical properties of an ice cover are determined by the stratification,
34 crystal structure, and gas bubbles and other impurities. They control ice mechanics, growth and decay
35 of ice, and transfer of sound and electromagnetic signals which have a key role in lake ice remote
36 sensing, under-ice living conditions, and ice ecology (Iliecu and Baker, 2007; Li et al., 2010; Shoshany
37 et al., 2002). Although most boreal lakes possess a seasonal ice cover, lake research has traditionally
38 focused on summer, and especially little is known about the ice decay period when the ice melts,
39 weakens, and disappears. The obvious reason is that fieldwork is then logistically very difficult.
40 However, the structure and properties of ice undergo rapid changes during the decay period that has an
41 important influence on the conditions in **and** below the ice cover.

42 There are two major practical problems with melting lake ice due to the loss of strength caused by
43 the ice deterioration (Ashton, 1985; Leppäranta, 2015; Masterson, 2009). First, the bearing capacity of
44 ice decreases, and therefore on-ice traffic becomes risky. Accidents are reported every spring due to the
45 weak ice, connected with fishing or crossing of lakes. Second, a weakened ice cover may be broken,
46 forced drifting by wind, and pushed onshore. Such ice with finite strength is a risk for structures near
47 the shore, such as docks and bridges, and may cause near-shore erosion. Hence, it is urgent to study the
48 physical properties of ice during the melting period.

49 The climatology of ice breakup date has been widely studied based on long-term time-series
50 records (Benson et al., 2012; Korhonen, 2006; Karetnikov et al., 2017; Magnuson et al., 2000). A steady
51 trend toward earlier melting date has been reported in most recent ice phenology studies, by about one
52 week over 100 years in boreal lakes, attributed to the global climate warming. Numerical modelling
53 studies of ice breakup have revealed that the time when ice starts to melt and internal melting of ice
54 have major impacts on the accuracy of the simulations (Yang et al., 2012). The timing of ice breakup is

55 a question of atmospheric warming and falling albedo (Leppäranta, 2014), and its proper solution
56 requires a quantification of the physical mechanisms that control the melting of ice.

57 The trend toward earlier breakup has been suggested as a driving factor to changes of ecological
58 and biogeochemical processes in seasonally ice-covered lakes (Garcia et al., 2019; Griffiths et al., 2017).
59 Lake ice interacts with the under-ice water body to further drive or facilitate the migration and
60 transformation of nutrients and metals, resulting in changes in the phytoplankton biomass (Cavaliere
61 and Baulch, 2018; Schroth et al., 2015). In addition, the ecosystem under the ice affects the limnology
62 of the following seasons (Hampton et al., 2017). pH, electrical conductivity, and chlorophyll *a* are
63 important indicators of the ecological environment and have significant impacts on the primary
64 production, but it is uncommon to see field data of them in the ice decay period. In general, the lack of
65 knowledge of the role of ice melting in ecological and biogeochemical processes limits the proper
66 assessment of the impact of climate change on cold region lakes (Tan et al., 2018).

67 Due to the difficult fieldwork conditions on deteriorating ice cover, there has not been much in situ
68 research during the ice decay period. A snow cover delays the melting by its high albedo and low
69 transmissivity of light (Ashton, 1986; Leppäranta, 2015; Warren, 1982). When the ice cover is
70 snow-free, sunlight penetrates to the ice and through the ice. The ice warms up and melts inside, the
71 under-ice water is heated, and the surface heat balance determines whether surface melting takes place
72 (Kirillin et al., 2012). Ice impurities are released from melting ice into the water that changes the water
73 environment. The under-ice light is also used for primary production, which normally peaks after ice
74 breakup.

75 The present knowledge of the melting rate of ice is limited to a few studies, showing typical values
76 of $1\text{--}3 \text{ cm d}^{-1}$ in terms of equivalent ice thickness. Melting takes place at the top and bottom boundaries
77 and in the interior depending on the weather conditions (Jakkila et al., 2009; Leppäranta et al., 2010,
78 2019; Wang et al., 2005). It has been found that the light transmittance changes with internal melting
79 that has influence on further melting. Internal melting also opens channels for flushing the ice by
80 surface meltwater and lake water. When the porosity of ice reaches the level of around 0.5, the ice cover
81 collapses by its own weight and disappears rapidly (Leppäranta et al., 2010, 2019). Bottom melting is

82 caused by the heat flux from water that can be large in spring due to the solar heating of the under-ice
83 water (Jakkila et al., 2009; Shirasawa et al., 2006).

84 We examine here the decay of ice in a boreal lake, Lake Pääjärvi, in southern Finland by field
85 surveys in two years, 2018 and 2022. The objective was to analyse the ice melting process for the
86 evolution of ice thickness and porosity as well as for the changes in ice and water geochemistry. The
87 structure and properties of ice experienced remarkable changes during the decay process, and
88 significant melting occurred in the surface and bottom and in the interior. Flushing of ice by meltwater
89 and lake water caused changes to ice and water geochemistry. A deeper knowledge of the ice decay is
90 needed for modelling the lake ice decay, particularly for ice engineering issues, and for understanding
91 the physical and geochemical conditions for ecology of freezing lakes in spring. This paper gives the
92 results of the Lake Pääjärvi field program.

93 **2 Materials and methods**

94 **2.1 Study site**

95 Lake Pääjärvi is located in the boreal zone in southern Finland ($61^{\circ}40' N$, $25^{\circ}08' E$). The lake area is
96 13.4 km^2 , the mean and maximum depths are 14.4 m and 87 m, respectively, and the catchment area is
97 244 km^2 (Arvola et al., 1996). Lake Pääjärvi is a humic, brown-water lake with an average optical depth
98 of 0.67 m and Secchi depth of 1.8 m (Arst et al., 2008). The decay of the ice cover takes about one
99 month, controlled by the presence of snow on top, the optical quality of snow and ice, and the
100 atmospheric and solar forcing (Wang et al., 2005; Jakkila et al., 2009). The LBS ice phenology data
101 base shows that in 1970–2022 the ice breakup date was on average April 25, with a standard deviation
102 of 12 days. In 1993–1999, the maximum annual ice thickness was on average 46 cm with the standard
103 deviation of 12 cm, and the fraction of snow-ice was on average one-third (Leppäranta and Kosloff,
104 2000).

105 The field study was made in Pappilanlahti Bay in the west side of the lake near the Lammi
106 Biological Station (LBS). The bay is shallow (maximum depth 12 m), with three small inflow brooks
107 and a weak groundwater flux at the bottom. The field site was about 100 m from the shore with access

108 first by foot and in late season by a hydrocopter and a boat. Our field program included a pilot study in
109 12–20 April 2018 and the main experiment in 25 March – 3 May 2022, which was more extensive and
110 provided the main body of the data. The ice situation was recorded by ground photographs, drone
111 orthophotos, and field notes, and ice and water samples were collected at regular field visits. In 2022 the
112 whole decay period was mapped while in 2018 just the last eight days of it.

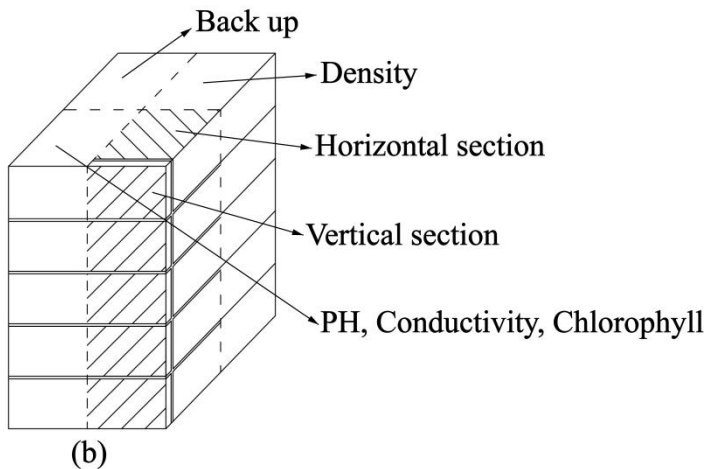
113 **2.2 Observations**

114 In the pilot study in 2018, the field site was visited five times between April 12 and April 20. The study
115 was focused on a short period at the end of the ice decay. Ice samples were taken on April 12, 15 and 20,
116 and thereafter, because of the rapid melting, it was not possible to walk on the ice or to use a boat for
117 sampling, but photographs were taken daily from the shore. Analyses of samples were made in similar
118 manner as in the main experiment (see below).

119 The study period in 2022 covered the whole decay period from March 25 to May 3 with eight field
120 site visits. The sampling was made by foot from the shore until April 22. Then an open water zone
121 formed at the shoreline, and a hydrocopter was used for ice sampling on April 26–29 (Fig. 1a). On May
122 3, the melting created several open channels, and a boat was used for the sampling. Each time the
123 quality and thickness of ice were recorded first with the freeboard, snow thickness, snow-ice thickness,
124 and congelation ice thickness measured by a ruler. Ice samples (cross-section 30 cm × 30 cm) were cut
125 by drill and saw, put in plastic bags, and transported immediately to a freezer (temperature –18 °C) in
126 LBS. Water samples were taken from the drill holes and stored in sealed bottles in a fridge at a
127 temperature of 4–6 °C.



128 (a)



128 (b)

129 **Figure 1.** Lake ice sampling and processing: (a) collect ice with a handsaw on the hydrocopter; (b) the ice block
 130 was sliced into four parts for different observations.

131 Available routine meteorological and hydrological data of the Finnish Meteorological Institute
 132 (FMI) and Finnish Environment Institute (SYKE) were utilized. The SYKE data include manual
 133 measurements of the thicknesses of ice, snow-ice and snow, and freeboard every ten days during the
 134 whole winter in Pappilanlahti Bay, and they were used for the all-season ice and snow thickness
 135 reference and control. FMI provided the meteorological data of an automated station in LBS yard half a
 136 kilometre from our lake site and solar radiation data for the closest radiation site in Jokioinen. The LBS
 137 data base was utilized for the long-term ice phenology and geochemistry of the lake and inflow brooks
 138 of the study bay.

139 **2.3 Laboratory work**

140 The ice samples were analysed in the INAR (Institute of Atmospheric and Earth Sciences, University of
 141 Helsinki) ice laboratory (-10°C). Each ice sample was divided into four sections. Section 1 was cut
 142 vertically into layers for the geochemistry analyses from meltwater in the water laboratory. Section 2
 143 was cut vertically and horizontally to map the ice crystal structure and study the gas bubbles by image
 144 analysis, and Section 3 was cut vertically to layers to measure the density of ice. Section 4 was stored as
 145 a backup (Fig. 1b).

146 The samples were cut into vertical sections of 8–10 cm height by a bandsaw, and horizontal
 147 sections were extracted at the vertical cuts. The size and distribution of gas bubbles in the ice were

148 observed under normal light (Deng et al., 2019). The sections were frozen on glass plates to be prepared
149 for thin sections, and the crystal structure of ice was obtained from the thin sections between crossed
150 polarizers (Langway, 1958). The mass/volume method was used to measure the ice density in the
151 laboratory, and the freeboard in the field was used as a control. The sample was cut into 5 cm cuboids
152 by a bandsaw. The sides of a cuboid were measured by a vernier caliper, and the mass was measured by
153 an electronic scale with the accuracy of 0.001 g. The accuracy of the density is estimated as 10 kg m^{-3}
154 determined by the accuracy of the volume measurement.

155 The water samples as well as the ice meltwater samples were analysed in the LBS water laboratory
156 for pH, electrical conductivity (EC) and chlorophyll *a* (Chl *a*). The ice geochemistry samples were first
157 cut in the ice laboratory into vertical sections based on the structure at intervals of 8–10 cm by a
158 bandsaw, melted in sealed bags, poured into sample bottles, and stored in a fridge (at 4–6 °C). pH and
159 EC were measured from unfiltered samples according to the standards in SFS-EN 27888 and SFS 3021
160 using a Thermo Orion 3-STAR Precision Benchtop pH meter (accuracy 0.01) and YSI 3200
161 conductivity sensor (accuracy 0.01 $\mu\text{S cm}^{-1}$). The Chl *a* concentration was measured from the light
162 absorbance at 665 and 750 nm wavelengths (Arvola et al. 2014).

163 3 Results

164 3.1 Ice structure

165 3.1.1 Ice structure in the pilot study 2018

166 In 2018, the ice decay period began at the end of March, and the final breakup took place on April 25.
167 The thickness of ice was 42 cm on March 30, and on April 12 it was 35 cm with 5.3 cm snow-ice and
168 29.7 cm congelation ice (Table 1). Snow-ice melted in less than eight days, and congelation ice melted
169 fast after April 15. On April 24, rain greatly accelerated the melting.

170 **Table 1.** Thickness of ice layers and freeboard in the melting phase (cm) and porosity (%) in April 2018, also
171 shown is the ratio of freeboard (Fb) to draft.

2018	Snow-ice	Congelation ice	Total ice	Porosity	Freeboard	Fb/draft
April 12	5.3	29.7	35.0	~ 0	3.0	0.094
April 13	4.7	29.3	34.0	x	3.0	0.097
April 14	3.3	28.7	32.0	x	2.0	0.067

April 15	2.7	28.3	31.0	x	2.0	0.069
April 20	0	20.3	20.3	25	x	x
April 25	0	0	0	x	0	x

172 3.1.2 Ice structure in the main experiment 2022

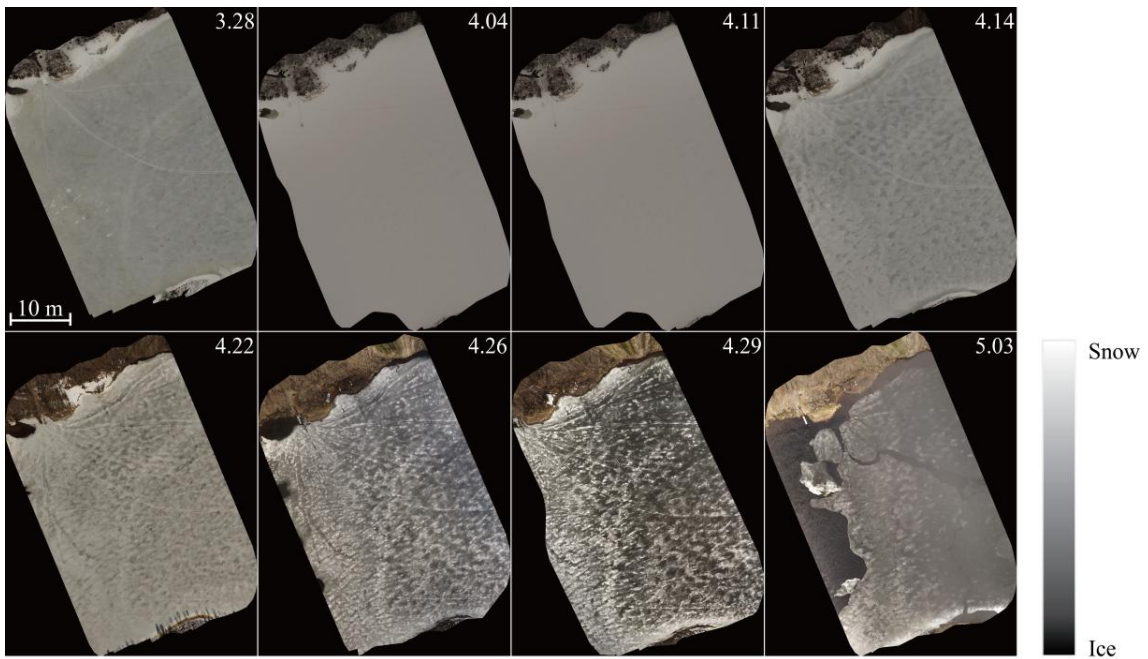
173 The ice decay period began on March 25 and the final breakup took place after 42 days on May 5
 174 (Table 2). The thickness of ice was 55 cm on March 25, close to the long-term mean, with 33 cm
 175 congelation ice and 22 cm snow-ice. During the decay period the ice was melting at both boundaries
 176 and in the interior. At the end of April there was a slush layer between the surface ice layer and the
 177 congelation ice layer with soft places so that walking on the ice was not easy.

178 **Table 2.** Thickness of ice layers and freeboard in the melting phase (cm) and porosity (%) in 2022, also shown is
 179 the ratio of freeboard (Fb) to draft. x stands for no data.

2022	Snow-ice	Congelation ice	Total ice	Porosity	Freeboard	Fb/draft	Snow
March 25	33	22	55	x	5.5	0.11	1
April 1	31	20	51	6.1	5	0.11	2.5
April 8	30	17	47	x	2	0.044	13
April 14	31	17	48	7.7	5	0.12	2
April 22	27	11	38	15.2	4	0.12	0
April 26	7.5 + 7 [¶]	10	24.5	17.1	1	0.043	0
April 29	6 + 12 [¶]	4	22	24.1	0.5	0.023	0
May 3	2	0	2	34.0	x	x	0
May 5	0	0	0	x	0	x	0

180 ¶ Surface ice + slush layer

181 Figure 2 shows drone orthophotos of the ice cover taken at an altitude of 100 m during the melting
 182 period. As reported by Ashton (1985) about melting lake ice in general, the ice cover of Lake Pääjärvi
 183 looked grayish and patchy from above. Snowfall turned the ice white at the beginning of April, and as
 184 the air temperature increased, the new snow began to melt creating a patchy surface. The positive
 185 albedo feedback of melting ice supports the persistence of surface patchiness.



186

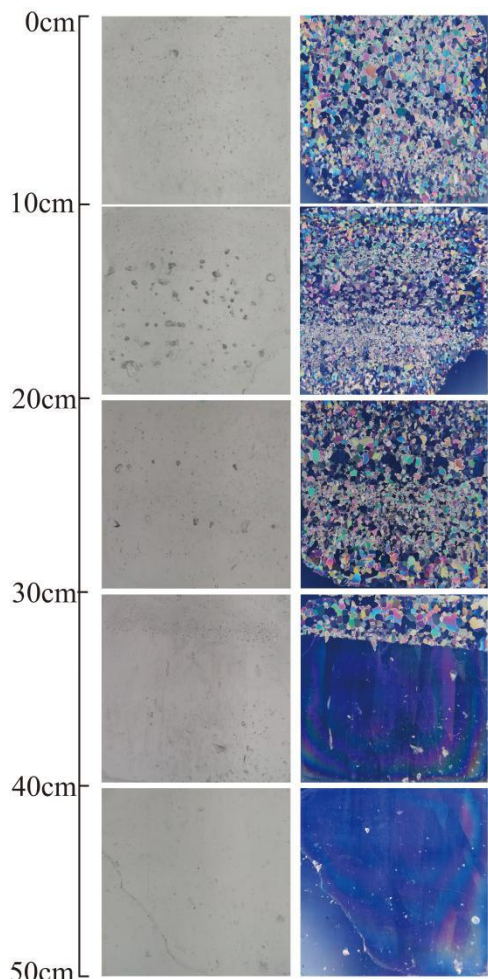
187 **Figure 2.** Drone orthophotos of the ice cover in the melting period in 2022 (time given as month.day).

188 There were two principle vertical layers in the Lake Pääjärvi ice cover (Fig. 3). The top layer was
 189 granular snow-ice, with the grain size of 1–9 mm and blurred crystal boundaries, and the lower layer
 190 was clear columnar congelation ice with the grain size of 2–10 cm. When the ice melting progressed,
 191 the ice crystal structure data showed that the thickness of both snow-ice and congelation ice decreased,
 192 and the porosity of ice increased.

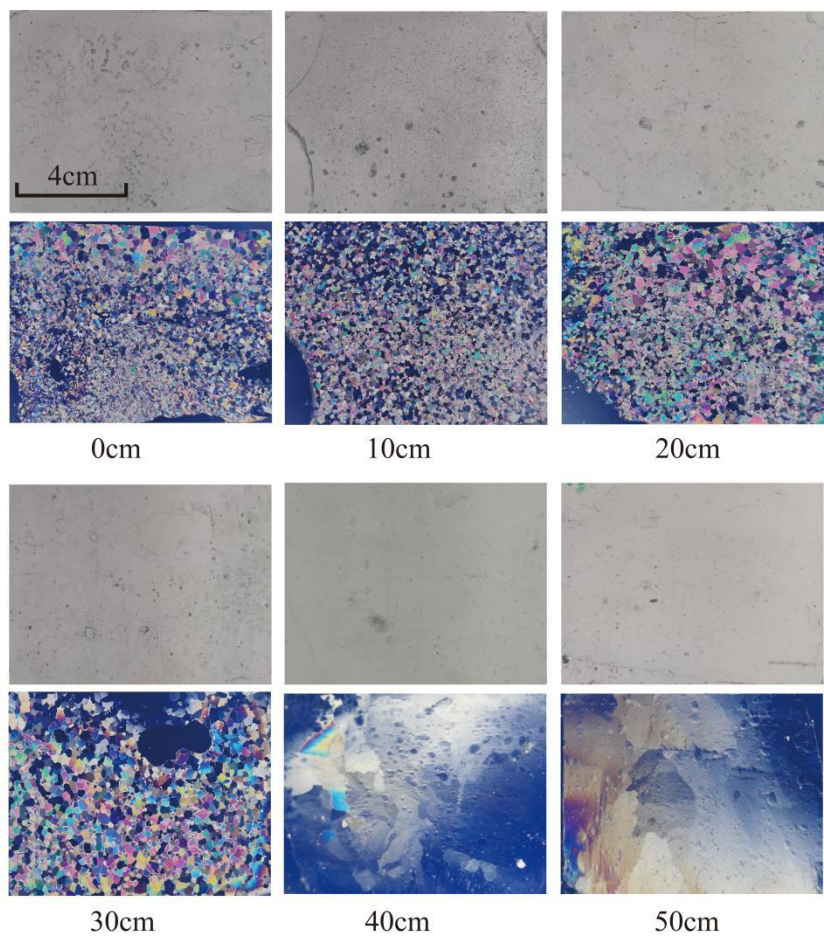
193 The ice melted 4 cm in May 25–April 1. On April 1, the snow-ice part had two sub-layers (Fig. 3).
 194 The top 27 cm sub-layer had very irregular crystal structure with blurred crystal boundaries and grain
 195 size mainly within 1–2 mm. In the lower, 27–31 cm, layer the crystals were granular with clear
 196 boundaries, and the grain size was mainly 2–5 mm. It was judged that the upper sub-layer had
 197 undergone thawing and refreezing process. The columnar ice layer underneath was clear ice with grain
 198 size increasing with depth, from 2 to 10 cm. The volume fraction of gas bubbles was 4–6 % in the
 199 snow-ice layer. They were cylindrical and spherical shaped with the maximum diameter of 4 mm. The
 200 corresponding fraction was 1–2 % in congelation ice, the bubbles were spherical with the maximum
 201 diameter of 1 mm.

202 In April 1–14 congelation ice melted by 3 cm, but snow-ice thickness was unchanged. According to
203 the weather data, a snowfall began on April 5, and then the air temperature rose resulting in the
204 formation of new snow-ice through the melt–freeze cycle. Compared with April 1, the ice crystal size
205 had not changed, and the gas volume of snow-ice was 5–7 %. After April 14, the air temperature
206 increased further, and the ice melted by 10 cm in April 14–22. The horizontal and vertical sections
207 showed strong melting at the grain boundaries in snow-ice (Fig. 4a). The gas content increased in
208 snow-ice to 6–10 % and in congelation ice to 1–3 %. Also, the maximum diameter of gas bubbles
209 increased to 5 mm in snow-ice and 3 mm in congelation ice.

210 In April 26–29, a slush layer appeared below a surface ice layer due to internal melting of ice (Fig.
211 4b). The columnar ice began to melt at crystal boundaries where gas inclusions appeared. On April 29,
212 the gas volume reached 5 % in the columnar layer, with the maximum bubble size equal to 5 mm. On
213 May 3, the columnar ice and slush layers had melted, and there was only 2 cm snow-ice left (Fig. 4c).

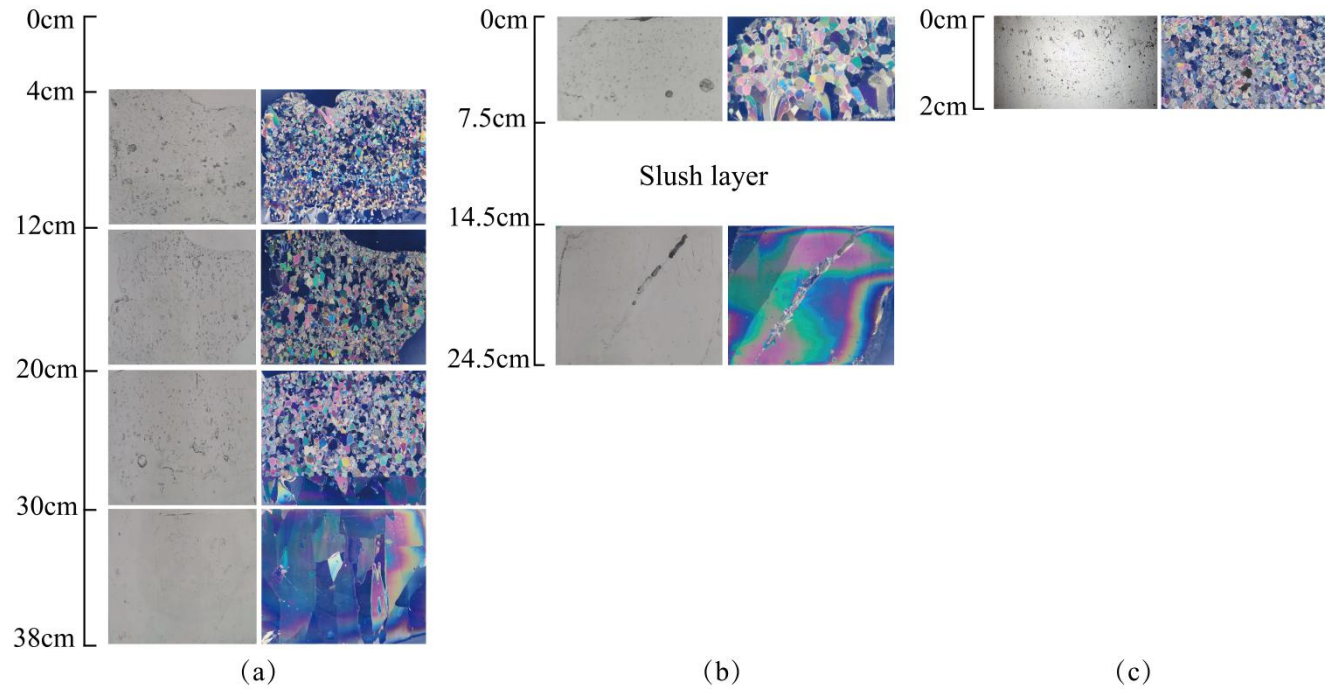


214 (a)



214 (b)

215 **Figure 3.** Lake Pääjärvi ice crystal structure of April 1. (a) vertical profiles under the normal light (left) and ice
216 crystal structure under the polarized light (right), (b) horizontal sections under the normal light (top) and ice
217 crystal structure under the polarized light (bottom).



218

(a)

(b)

(c)

219 **Figure 4.** Lake Pääjärvi ice crystal structure of April 22, April 26, and May 3. (a) vertical profiles under the
 220 normal light (left) and ice crystal structure under the polarized light (right) on April 22; (b) vertical profiles
 221 under the normal light (left) and ice crystal structure under the polarized light (right) on April 26; (c) vertical
 222 profiles under the normal light (left) and ice crystal structure under the polarized light (right) on May 3.

223 **3.1.3 Ice melt rate**

224 The ice sample data in Tables 1–2 were used to estimate the melting at the surface and bottom and
 225 in the ice interior. The melting rate increased toward the breakup date. In 2018 the ice cover was
 226 different from 2022 in that the ice was mostly (85 %) congelation ice (Table 1). In April 12–20 the
 227 mean surface and bottom melting together was 1.84 cm d^{-1} , and the mean internal melting was 0.86 cm
 228 d^{-1} . In April 12–15 the mean surface and bottom melting were 0.87 cm d^{-1} and 0.47 cm d^{-1} , respectively.
 229 The ice was more transparent than in 2022 that allowed more sunlight penetration through ice. The
 230 bottom melting in 12–15 April corresponded to the heat flux

231
$$Q = \frac{\rho_i L_f \Delta h}{\Delta t} = 16 \text{ W m}^{-2} \quad (1)$$

232 where ρ_i is ice density, L_f is the latent heat of freezing, Δh is the change in ice thickness, and $\Delta t =$
 233 1 d.

234 **Table 3.** Ice melting in spring 2018 (cm). The numbers show the change from the row above to the present one.
 235 At the end, surface melting and bottom melting cannot be separated from the data as shown by z1 and z2. x is for
 236 no data.

2018	Surface melt	Bottom melt	Total melt	Internal melt
April 12	0	0	0	0
April 13	0.6	0.4	1.0	x
April 14	1.4	0.6	2.0	x
April 15	0.6	0.4	1.0	x
April 20	2.7+ z1	8.0- z1	10.7	6.9
April 25	z2	20.3- z2	20.3	x

237 In 2022 the mean rate was 1.31 cm d^{-1} , and snow-ice melted a little faster than congelation ice. The
 238 mean melt rates were, respectively, 0.79 cm d^{-1} and 0.38 cm d^{-1} . There was a minor new snow-ice
 239 formation on April 14, and the last 2 cm thick piece was snow-ice on May 3. The mean melt rate at the
 240 bottom corresponds to the heat flux of 13 W m^{-2} from water to ice. This flux was larger than normally
 241 assumed (e.g., Yang et al., 2012). The mean internal melt rate was 0.18 cm d^{-1} equivalent ice thickness
 242 that was smaller than the surface and bottom melting, attributed to the low light transmittance of
 243 snow-ice. In the last week of melting, the ice was highly porous and internal breakages occurred.

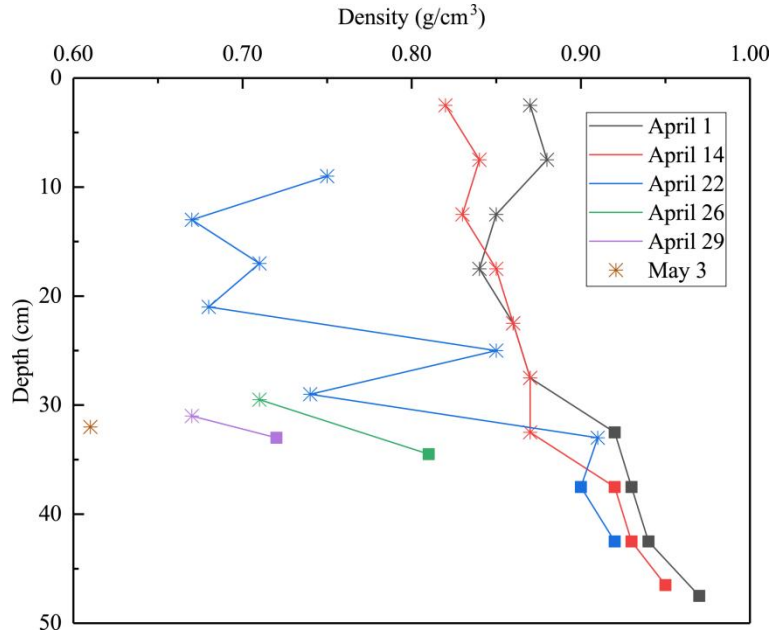
244 **Table 4.** Ice melting in spring 2022 (cm). The numbers show the change from the row above to the present one.

2022	Surface melt	Bottom melt	Total melt	Internal melt
March 25	0	0	0	0
April 1	2	2	4	x
April 8	1	3	4	0.4
April 14	-1	0	-1	0.4
April 22	4	6	10	3.2
April 26	4.5	1	5.5	0.6
April 29	4.5	6	10.5	1.6
May 3	16	4	20	1.2
May 5	2	0	2	0
Sum	33	22	55	7.4

245 3.2 Ice density

246 At the initial stage of melting, April 1–14, 2022, the estimated average densities of snow-ice and
 247 congelation ice were 850 kg m^{-3} and 930 kg m^{-3} , respectively. The congelation ice data are from the
 248 deep layers, and the apparently high density is likely due to liquid water in pores. The density profiles
 249 shifted toward lower level with time while the density always increased with depth (Fig. 5). On April 22

250 the snow-ice density was higher than on April 14 at large depth that can be due to meltwater
 251 accumulation in deep pores. Toward the ice breakup, the density decreased, in snow-ice to below 700
 252 kg m⁻³ and in congelation ice to almost 700 kg m⁻³. The density data were used to estimate the porosity,
 253 which was found to increase from 6.1 % to 34 % during the melting period (Table 2).



254 **Figure 5.** Lake Pääjärvi ice density profiles in 2022 (asterisk stands for snow-ice, square for congelation ice).

255 For bare ice, the freeboard/draft ratio is

$$257 \quad \frac{h_f}{h_d} = \frac{\rho_w - \rho_d}{\rho_f} \quad (2)$$

258 where h is thickness and ρ is density, and the subscripts are w for water, d for draft, and f for
 259 freeboard. In winter, for $\rho_f \approx \rho_d \approx 910$ kg m⁻³, this ratio is 0.10. It increases when the porosity
 260 decreases evenly, but it decreases if meltwater drainage from freeboard is trapped inside the draft to
 261 reduce the buoyancy. This is consistent with the present field observations.

262 3.3 Heat budget

263 We consider the volume of ice per unit area (V), expressed by the ice thickness (h) and porosity (ν)
 264 as $V = (1 - \nu)h$. The external heat fluxes include the surface flux Q_0 , the heat flux from water to ice

265 bottom Q_w , and the absorption of solar radiation inside ice Q_A . It is assumed that in the melting stage
 266 the ice is isothermal with the temperature at the melting point. The heat fluxes are taken positive toward
 267 the ice, and for simplicity negative fluxes are ignored, i.e., the model heat flux is $Q_0^+ = \max(Q_0, 0)$.
 268 The surface and bottom fluxes reduce the thickness of ice, while the internal heating increases the
 269 porosity. Thus, we have (Leppäranta et al., 2019)

$$270 \quad \rho_i L_f (1 - \nu) \frac{dh}{dt} = - (Q_0^+ + Q_w) \quad (3a)$$

$$271 \quad \rho_i L_f h \frac{d\nu}{dt} = Q_A \quad (3b)$$

272 At $\nu = \nu^* \sim 1/2$, the ice breaks due to its own weight and the remaining ice pieces melt fast.

273 Here the surface heat flux is based on air temperature due to the lack of more complete atmospheric
 274 observations. The linearized approximate formula of Leppäranta (2015) is employed:

$$275 \quad Q_0 = k_0(t) + k_1(T_a - T_0) \quad (4)$$

276 where k_0 is independent of the surface temperature but depends on time, and $k_1 \sim 15 \text{ W m}^{-2} \text{ }^\circ\text{C}^{-1}$. In
 277 exact terms, k_0 includes the radiation balance and latent heat flux at $T_a = T_0$, and their correction for
 278 $T_a \neq T_0$ plus the sensible heat flux is included in k_1 . In Lake Pääjärvi, k_0 varies between -50 W m^{-2}
 279 and 115 W m^{-2} in summer (Leppäranta and Wen, 2022). The second term in Eq. (4) represents the
 280 common degree-day model of ice melting, while the first term is geographic representing the location
 281 (Leppäranta and Wen, 2022). The given value of k_1 corresponds to the degree-day coefficient of 0.43
 282 $\text{cm } (\text{ }^\circ\text{C} \cdot \text{d})^{-1}$, which is close to the usual degree-day coefficient in hydrological forecasting (Leppäranta,
 283 2015).

284 The internal melting and bottom melting depend on the solar radiation. We have (see Leppäranta et
 285 al., 2019)

$$286 \quad Q_A = (1 - \alpha) \gamma (1 - e^{-\lambda h}) Q_{s0} \quad (5)$$

$$287 \quad Q_w = Q_{w0} + c(1 - \alpha) \gamma e^{-\lambda h} Q_{s0} \quad (6)$$

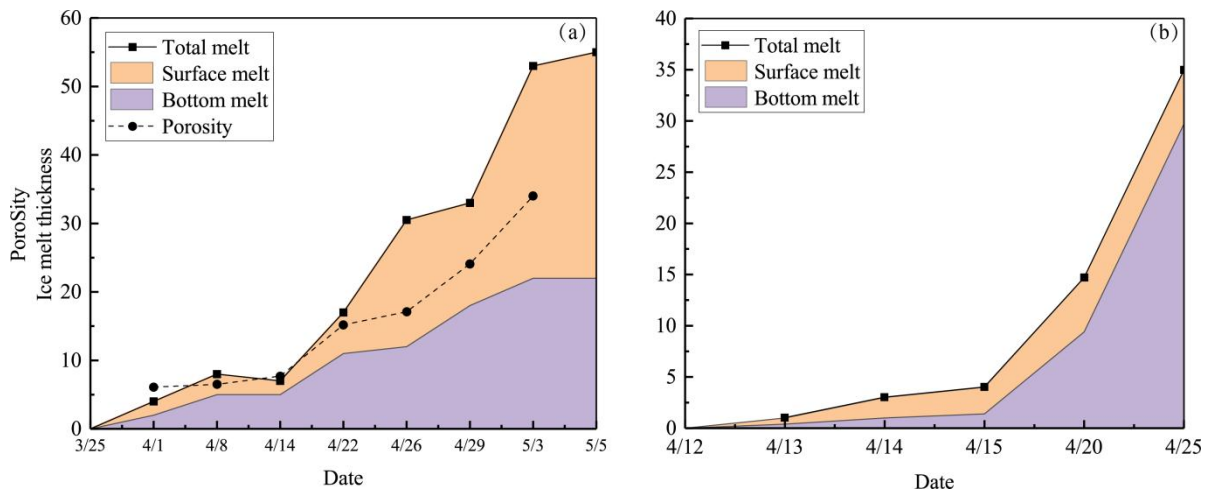
288 where α is albedo, $\gamma \approx 0.5$ represents the fraction of solar radiation that penetrates the surface (the
 289 light band), λ is the light attenuation coefficient, and c is the fraction of under-ice solar heating

290 returning to ice bottom. Eq. (5) gives the part of solar radiation used for internal melting, and the bottom
291 melting in Eq. (6) consists of the background heat flux from the deep water (Q_{w0}) and a part of the
292 under-ice solar radiation.

293 The heat fluxes for ice melting in 2022 were estimated from Eqs. (4-6). The forcing was provided
294 by the solar radiation data of FMI station Jokioinen and by the air temperature data of FMI station
295 Lammi. It was assumed that the surface temperature was at the melting point. The incident solar
296 radiation averaged to 126 W m^{-2} in the last week of March and 198 W m^{-2} in the first week of May, and
297 the maximum daily average was 268 W m^{-2} , on April 25. The albedo was parameterized as $\alpha = 0.7$ for
298 snow, 0.5 for dry ice and 0.3 for wet ice, and $\lambda = 0.5 \text{ m}^{-1}$ was fixed. The mean solar radiation and the
299 mean air temperature were 184 W m^{-2} and $2.4 \text{ }^{\circ}\text{C}$ in April 2022, while the corresponding climatological
300 values are 152 W m^{-2} and $3.5 \text{ }^{\circ}\text{C}$.

301 The function k_0 was estimated based on Leppäranta (2015): k_0 increased from -35 W m^{-2} on
302 March 25 to -1 W m^{-2} on May 5. The total modelled surface melting became 36.6 cm, which is rather
303 close to the observation (33 cm) obtained from the ice structure analysis (Table 3). The resulting mean
304 absorption of solar radiation by ice was $Q_A = 5.6 \text{ W m}^{-2}$ corresponding to the melt rate of 0.16 cm d^{-1} ,
305 close to 0.18 cm d^{-1} obtained from the ice structure data. To evaluate the heat flux from the water, we
306 took $c = 0.3$ (Leppäranta et al., 2019), and then the contribution of solar radiation to the heat flux to ice
307 bottom became 10.5 W m^{-2} . The background term Q_{w0} is not known but for molecular conduction the
308 scale is $Q_{w0} = k_w \partial T / \partial z \sim 1 \text{ W m}^{-2}$, where $k_w = 0.56 \text{ W m}^{-1} \text{ }^{\circ}\text{C}^{-1}$ is thermal conductivity of water,
309 and in general mid-winter data suggest that $Q_{w0} < 5 \text{ W m}^{-2}$. With $Q_{w0} = 1 \text{ W m}^{-2}$, we have $Q_w =$
310 11.5 W m^{-2} and the corresponding melt rate at the ice bottom would be 0.33 cm d^{-1} . This result is
311 supported by the estimate $Q_w = 13 \text{ W m}^{-2}$ from the ice structure data in Section 3.1.

312 Ice melting obtained from the ice structure data is illustrated in Fig. 6. In 2022, the surface melting
313 was greater than the bottom melting, while in 2018, it was the opposite. The main reason for this
314 difference was in the ice stratification. In 2022, the snow-ice layer accounted for 60 % of the ice cover,
315 while in 2018, the fraction was only 15 %. The melting rate was gradually increasing with the weather
316 getting warmer and solar radiation increasing with time.



317

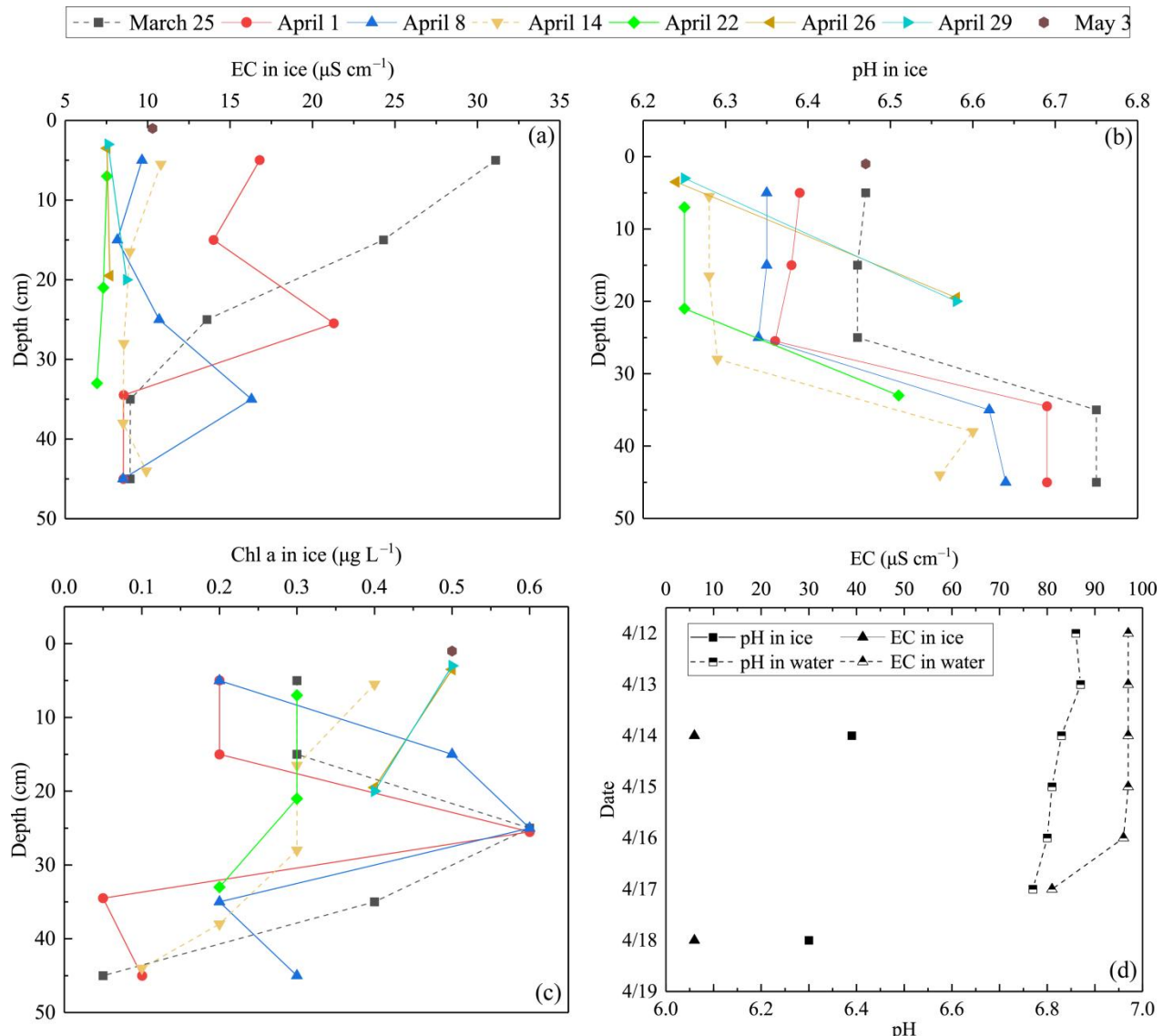
318 **Figure 6.** Accumulated ice melting and porosity in 2022 (left) and 2018 (right) based on field data of ice
319 structure. Porosity was not recorded in 2018.

320 3.4 Ice geochemistry

321 During the ice decay period, meltwater was mixed into the under-ice water layer that influenced the
322 water geochemistry. In the present data the meltwater had lower pH and EC than the lake water (Figs.
323 7–8). On April 1, 2022, the mean pH and EC of snow-ice were 6.38 and 17.3 $\mu\text{S cm}^{-1}$, respectively, and
324 in congelation ice the corresponding values were 6.75 and 9.0 $\mu\text{S cm}^{-1}$. Atmospheric deposition of
325 acidic substances was judged as the background for the low pH of snow-ice. Then pH and EC decreased.
326 The vertical profiles of EC, pH and Chl *a* show that EC was larger near the snow-ice surface than in
327 congelation ice in the early melting stage, but the difference was no more obvious after April 14. pH
328 was always smaller in snow-ice than in congelation ice. Chl *a* content was less than 0.6 $\mu\text{g L}^{-1}$ with the
329 maximum at the snow-ice–congelation ice interface. In 2018, the limited data showed that EC was 6 μS
330 cm^{-1} and pH was 6.35 in ice.

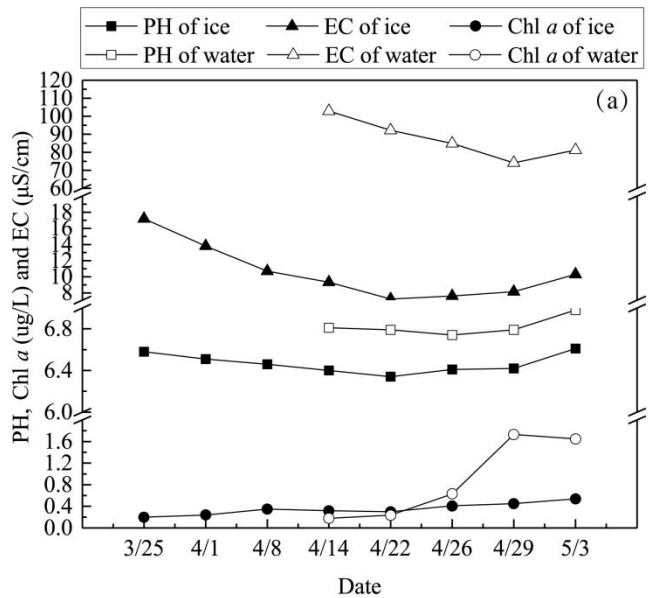
331 In lake water, the mean \pm standard deviation of pH and EC were 6.82 ± 0.09 and $92.5 \pm 12.7 \mu\text{S}$
332 cm^{-1} , respectively, in 2022. EC was smaller in ice by one order of magnitude than in water, on average
333 $\text{EC(ice)} = 0.12 \cdot \text{EC(water)}$. EC was decreasing with time in water due to meltwater drainage from ice
334 (Fig. 8). The changes in pH and EC had both signs, caused by flushing by meltwater and lake water. pH
335 increased in the late melting period after the slush layer appeared, likely due to the increase in the

336 photosynthesis enhanced CO₂ consumption. However, the inflow from brooks into the study bay could
 337 cause an opposite effect (Fig. 9). The inflow was weak until April 21, but in April 21–25 it
 338 corresponded to 17 % of the water volume of the bay.



339

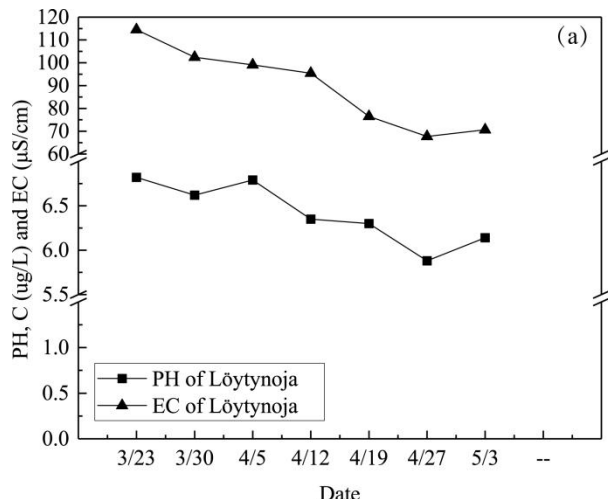
340 **Figure 7.** EC, pH and Chl *a* in ice meltwater and under-ice water at the study site in 2022 and 2018. (a) EC in ice
 341 meltwater and under-ice water at the study site in 2022; (b) pH in ice meltwater and under-ice water at the study
 342 site in 2022; (c) Chl *a* in ice meltwater and under-ice water at the study site in 2022; (d) EC and pH in ice
 343 meltwater and under-ice water at the study site in 2018.



344

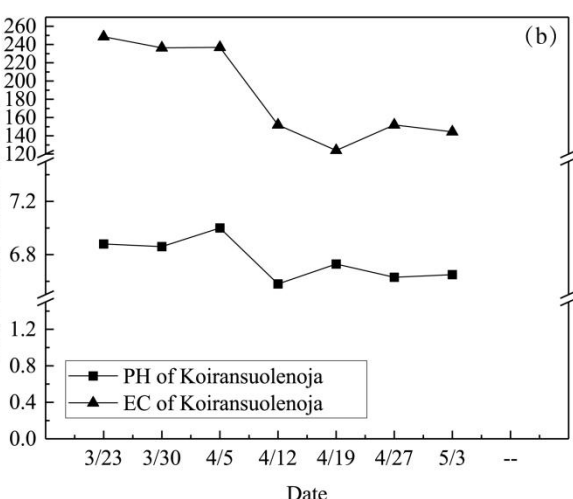
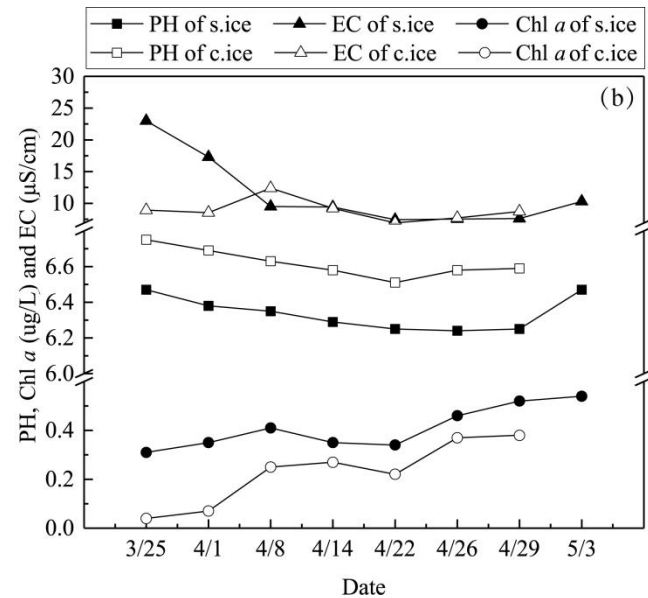
345 **Figure 8.** The mean pH, EC and Chl *a* in ice and lake water in 2022 (left) and the mean pH, EC and Chl *a* in
 346 snow-ice (s.ice) and congelation ice (c.ice) (right).

347 Algae can grow under ice and in slush layers in ice all winter at sufficient photon flux conditions.
 348 In springtime algae growth occurs also in pores in ice containing liquid water. Chl *a* content was similar
 349 in under-ice water and in ice until April 26, but then it increased in water and became much higher than
 350 in ice at the time of ice breakup, but still well below the first summer peak.



351

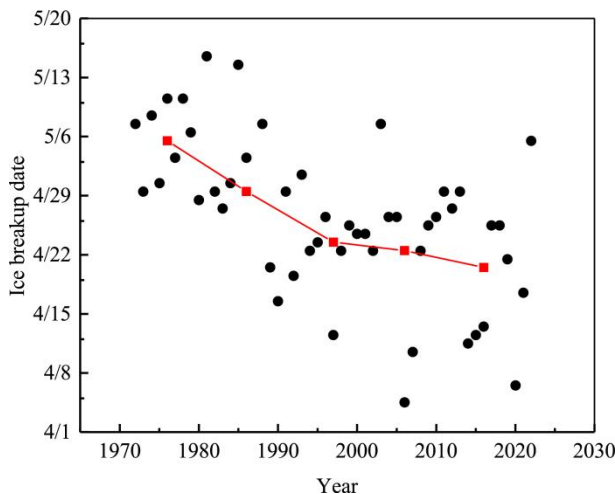
352 **Figure 9.** pH and EC in two inflow brooks, Löytynoja (left) and Koiransuolenoja (right), to the Pappilanlahti
 353 Bay.



355 **4.1 Interannual variations of ice breakup date**

356 Field data of lake ice are very important to examine and predict ice phenology and the ice break up date
357 is an significant ice phenological parameter during ice melting period (George, 2007; Williams et al.,
358 2004; Stefen and Fang 1997). Based on the ice break data from the Lammi Biological Station, we can
359 see the interannual variations of ice breakup date in a boreal lake, Pääjärvi. The date of ice breakup is
360 largely affected by solar radiation and the thickness and structure of ice and snow layers. Snow cover
361 blocks the atmospheric and solar heat fluxes to the ice and prevents deterioration of the ice under snow.
362 The first critical time in ice decay is the snow melting. Due to the positive albedo feedback and
363 increasing solar radiation, it is difficult to pause melting. The melt rate of ice is $1\text{--}3\text{ cm d}^{-1}$, increasing
364 with time.

365 The ice breakup date has become earlier in the last 50 years in Lake Pääjärvi, but the interannual
366 variability has been large (Fig. 10). In 1970–1990 the change was about 5 days per decade that is more
367 than can be explained by the regional warming, and the reason remains unclear. In general, in southern
368 Finland the trend of the breakup date is 0.5–1 day earlier per decade as is typical in the global scale
369 (Bernhardt et al., 2011; Magnuson et al., 2000). In northern Finland, Lake Kilpisjärvi, the trend from
370 1964 to 2008 was 0.44 days over a decade towards earlier ice breakup (Lei et al., 2012). Earlier ice
371 breakup has a potentially widespread implications on 50 countries (Sharma et al., 2019). The loss of
372 lake ice may lead to a reduction in the availability of fresh water due to increased evaporation, as well
373 as to cultural and socio-economic impacts to lake ice recreation, such as ice fishing and skating.



374

375 **Figure 10.** The ice breakup date of Lake Pääjärvi in 1970–2022. The black dots show the breakup date and the
 376 red squares show the ice breakup date averaged in every 10 years. Data source: Lammi Biological Station.

377 4.2 Comparisons of ice melting with other lakes

378 Melting of ice begins when the heat balance turns positive in spring and takes place at the surface,
 379 interior and bottom depending on the ice structure and fluxes. In 2022, the mean melting rate was 0.79
 380 cm d^{-1} at the surface, 0.52 cm d^{-1} at the bottom, and 0.18 cm d^{-1} in the ice interior in Lake Pääjärvi. In
 381 an Arctic tundra lake in northern Finland, Lake Kilpisjärvi, the triple (surface, bottom, and internal
 382 melting) was $(2.9, 0.5, 1.0) \text{ cm d}^{-1}$ in a warm spring 2013 and $(0.8, 0.1, 1.0) \text{ cm d}^{-1}$ in a normal spring
 383 2014 (Leppäranta et al., 2019). In a boreal lake, Lake Vendyurskoe, at $61\text{--}62^\circ\text{N}$, field investigations in
 384 two seasons showed the mean melt rates of 1.2 cm d^{-1} at the surface in both cases and 0.8 and 0.2 cm
 385 d^{-1} at the bottom (Leppäranta et al., 2010). **The differences in the quality of melting are due to**
 386 **differences in the congelation ice/snow-ice fractions and weather conditions that determine the level of**
 387 **light transfer through ice and surface heat balance.**

388 The porosity of ice needs to be estimated to examine the internal melting process. In the present
 389 work, the porosity was estimated from the measured ice density directly and from the absorbed solar
 390 radiation indirectly. The results were consistent with each other. Increasing porosity during the melting
 391 period changes the ice structure and decreases the strength of ice, and finally leads to breakage with
 392 rapid final disappearance of ice. Here the breakage took place in May 3–5 when the porosity of the ice

393 was 40–50 %. Leppäranta et al. (2019) used the solar radiation method to evaluate the porosity and
394 found the same level at the breakage **supporting our result**.

395 The heat flux from the lake water body to the bottom of ice has not been much studied (Shirasawa
396 et al., 2006; Kirillin et al., 2012). A heat flux of the order of 1 W m^{-2} represents molecular conduction
397 in the near-surface water layer and may be feasible in mid-winter (e.g., Jakkila et al., 2009; Kirillin et
398 al., 2012; Yang et al., 2012), but in spring, penetration of solar radiation to the water body gives a
399 fractional return flux to the ice bottom. According to the present study, the heat flux from water to ice
400 scales as 10 W m^{-2} in melting period, and the more transparent ice allowed more sunlight penetration
401 and larger heat flux. Jakkila et al. (2009) reported the heat flux values in Lake Pääjärvi as 12 W m^{-2}
402 during the final stage of ice melting that is very close to the present results, while Leppäranta et al.
403 (2019) obtained $15\text{--}20 \text{ W m}^{-2}$ in a warm spring but less than 5 W m^{-2} in a normal spring in a tundra
404 lake. In the earlier literature, smaller values have been reported even at late stages of ice melting. E.g.,
405 Bengtsson et al. (1996) obtained this heat flux ranging within $5\text{--}7 \text{ W m}^{-2}$ in March–April in small
406 Swedish lakes. **Thus the picture of increasing bottom melting is clear, but the question anyway** remains
407 the most uncertain component of the heat budget of lake ice, and more research is needed (Kirillin et al.,
408 2018).

409 The quality of ice decay is important to ice mechanics due to the loss of ice strength (Ashton, 1986;
410 Leppäranta, 2015). There are two important consequences. First, the bearing capacity of ice (P)
411 decreases. This quantity scales as $M \propto \sigma_f h^2$, where σ_f is the flexural strength, and during the melting
412 period ice thickness and strength both decrease, thickness due to melting at the boundaries and strength
413 due to internal melting. The positive albedo feedback in the melting process produces a patchy ice cover,
414 and together with the unpredictable bearing capacity the ice cover becomes a severe safety issue.
415 Secondly, the two-dimensional yield strength of a lake ice cover scales as $P \propto \sigma_c h/L$, where σ_c is the
416 compressive strength of ice and L is the lake size length scale. With decreased thickness and strength,
417 wind stress may lead to ice breakage and ice movement on shores, where damage can be caused to
418 man-made structures since the ice strength is still finite.

419 **4.3 Ice melting impact on geochemistry**

420 Porous melting ice is permeable to water. Meltwater can flow down from top and lake water may
421 penetrate to pores from below that also influences the stratification of the under-ice water layer. Here
422 the basic geochemical properties were studied: pH, EC and Chl *a*. They provide information about
423 physical and chemical processes. The meltwater has lower EC than the lake water and, consequently, a
424 lower density, and therefore a thin fresh surface layer may form just under the ice (Kirillin et al., 2012).
425 The geochemistry also affects the physiological state of aquatic organisms, which will guide and predict
426 the changes of biological structure in the water during the melting season.

427 The geochemistry under melting ice has been rarely reported. Lake Pääjärvi was studied for ice and
428 water geochemistry in mid-winter in 1996–1998 (Leppäranta et al., 2003). Their mean EC in ice and
429 water were close to our data, 16.5 and 108 $\mu\text{S cm}^{-1}$, respectively, as compared with our 9.0 $\mu\text{S cm}^{-1}$ for
430 congelation ice, 17.3 $\mu\text{S cm}^{-1}$ for snow-ice, and 92.5 $\mu\text{S cm}^{-1}$ for water; their mean EC in snow was 13
431 $\mu\text{S cm}^{-1}$. In Leppäranta et al. (2003), pH was 6.7 for ice and 6.6 for water, but in our data, pH was a
432 little lower in snow-ice and congelation ice than in lake water. Chl *a* was less than 0.5 $\mu\text{g L}^{-1}$ in ice and
433 between 0.2 and 1.7 $\mu\text{g L}^{-1}$ in water which is of the same order of magnitude reported by previous
434 research (Leppäranta et al., 2003; Vehmaa and Salonen, 2009). Leppäranta et al. (2003) reported Chl *a*
435 in ice also less than 0.5 $\mu\text{g L}^{-1}$ in Lake Pääjärvi but about 3 $\mu\text{g L}^{-1}$ in a hypereutrophic lake 100 km
436 from Pääjärvi. The present results are consistent with the previous studies, the small differences can be
437 explained by the differences in the quality of winters.

438 **5 Conclusions**

439 Ice season has a specific role in the local environment and human life, and it has an impact on the lake
440 ecology far beyond the ice period. Research of lake ice has largely increased to evaluate the impact of
441 the predicted climate change on the ice phenology and properties. During the melting period, it is
442 difficult to do fieldwork due to the deterioration of the ice cover, and therefore only few data have been
443 collected. In the present work, ice decay was monitored from the start to the final breakup resulting with
444 a full time-series of the evolution of ice thickness, structure, and geochemical properties.

445 In 2022, the maximum thickness of ice was 55 cm with 60 % snow-ice, and in 42 days the ice
446 melted by 33 cm from the surface and 22 cm from the bottom while the porosity increased from less
447 than 5 % to 40–50 % at breakup. The comparison between ice structure and heat budget gave a good
448 agreement in quantifying the deterioration of the ice cover. This result is promising when considering
449 the possibility of detailed numerical modelling of ice deterioration. The largest uncertainty is in the
450 bottom melting, where more research is needed on under-ice boundary layer dynamics. Solar radiation
451 penetrating through ice adds a major contribution to the heat flux from water to ice, according to the
452 present results on the order of 10 W m^{-2} , which is significantly higher than usually assumed in lake ice
453 modelling.

454 Ice and water pH and EC decreased during the ice decay but experienced fluctuations due to
455 flushing by meltwater and lake water. The mean EC of ice was $11.4 \mu\text{S cm}^{-1}$, equal to the fraction 0.12
456 of the lake water EC. The mean ice pH was 6.44, lower by 0.4 than in water. Chl *a* in ice increased to
457 $0.6 \mu\text{g L}^{-1}$ in the late part of ice decay, with the maximum in the slush sub-layer of snow ice. At the end
458 of the decay, Chl *a* was $1.7 \mu\text{g L}^{-1}$ in water, still far from the first summer maximum.

459 The results are important for modelling the lake ice season and the annual cycle of lakes. Lake ice
460 has an important role in the physical, chemical, and ecological cycle, and these cycles are sensitive to
461 climate changes. For the ice melting season, detail modelling of the ice strength and the consequent
462 bearing capacity and ice forces has a major importance for the local societies in lake regions.

463

464 *Data availability.* The routine meteorological and hydrological data are available at:
465 <https://www.syke.fi> and <https://www.fmi.fi>. The ice samples data applied in this work can be accessed
466 by the link: <https://doi.org/10.5281/zenodo.7342770>.

467 *Author contributions.* YZ conceived the field and laboratory study in 2022 with ML and MF and wrote
468 the paper with contributions from JL and ZL. SS and JA performed the study in 2018. All co-authors
469 discussed the results and edited the manuscript.

470 *Acknowledgements.* We are grateful to the Lammi Biological Station and the Institute of Atmospheric
471 and Earth Sciences, University of Helsinki for providing logistical help and laboratories. Thanks to
472 Esa-Pekka Tuominen, Joni Uusitalo and Riitta Ilola for helping in the fieldwork and laboratory, and to

473 Lauri Arvola for comments on the manuscript. This work was financially supported by the National
474 Key Research and Development Program of China (Grant No. 2019YFE0197600), the National Natural
475 Science Foundation of China (Grant No. 52211530038) and the Academy of Finland (350576 and
476 333889), and a personal grant to Yaodan Zhang by China Scholarship Council (CSC).

477 *Competing interests.* The authors declare that they have no conflict of interest.

478 **References**

479 Arst, H., Erm, A., Leppäranta, M., and Reinart, A.: Radiative characteristics of ice-covered freshwater and brackish water
480 bodies, *Proc. Estonian Acad. Sci. Geology*, 55(1), 3–23, 2006.

481 Arst, H., Erm, A., Herlevi, A., Kutser, T., Leppäranta, M., Reinart, A., and Virta, J.: Optical properties of boreal lake waters
482 in Finland and Estonia, *Boreal Environ. Res.*, 13, 133–158, 2008.

483 Arvola, L., Kankaala, P., Tulonen, T., and Ojala, A.: Effects of phosphorus and allochthonous humic matter enrichment on
484 metabolic processes and community structure of plankton in a boreal lake (Lake Pääjärvi), *Can. J. Fish. Aquat. Sci.*, 53,
485 1646–1662, <https://doi.org/10.1139/f96-083>, 1996.

486 Arvola, L., Salonen, K., Keskitalo, J., Tulonen, T., Järvinen, M., and Huotari, J. : Plankton metabolism and sedimentation in
487 a small boreal lake—a long-term perspective, *Boreal Environ. Res.*, 19, 83–96, 2014.

488 Ashton, G. D.: Deterioration of floating ice covers, *J. Energy Resour. Technol.-Trans. ASME*, 107, 177–182,
489 <https://doi.org/10.1115/1.3231173>, 1985.

490 Ashton, G. D. (Ed.): *River and lake ice engineering*, Water Resources Publications, Littleton Colorado, 1986.

491 Benson, B. J., Magnuson, J. J., Jensen, O. P., Card, V. M., Hodgkins, G., Korhonen, J., Livingstone, D. M., Stewart, K. M.,
492 Weyhenmeyer, G. A., and Granin N. G.: Extreme events, trends, and variability in Northern Hemisphere lake-ice
493 phenology (1855–2005), *Climate Change*, 112, 299–323, <https://doi.org/10.1007/s10584-011-0212-8>, 2012.

494 Bengtsson, L., and Svensson, T.: Thermal regime of ice covered Swedish lakes, *Hydrol. Res.*, 27, 39–56, 1996.

495 Bernhardt, J., Engelhardt, C., Kirillin, G., and Matschullat, J.: Lake ice phenology in Berlin–Brandenburg from 1947–2007:
496 observations and model hindcasts, *Climatic Change*, 112, 791–817, <https://doi.org/10.1007/s10584-011-0248-9>, 2012.

497 Cavaliere, E., Baulch, H. M.: Denitrification under lake ice, *Biogeochemistry*, 137, 285–295,
498 <https://doi.org/10.1007/s10533-018-0419-0>, 2018.

499 Deng, Y., Li, Z. K., Li, Z. J., and Wang, J.: The experiment of fracture mechanics characteristics of Yellow River ice, *Cold
500 Reg. Sci. Tech.*, 168, <https://doi.org/10.1016/j.coldregions.2019.102896>, 2019.

501 Ellis, A. W., and Johnson, J. J.: Hydroclimatic analysis of snowfall trends associated with the North American Great Lakes, *J.
502 Hydrol.*, 5, 471–486, [https://doi.org/10.1175/1525-7541\(2004\)005<0471:HAOSTA>2.0.CO;2](https://doi.org/10.1175/1525-7541(2004)005<0471:HAOSTA>2.0.CO;2), 2004.

503 Garcia, S. L., Szekely, A. J., Bergvall, C., Schattenhofer, M., and Peura, S.: Decreased snow cover stimulates under-ice
504 primary producers but impairs methanotrophic capacity, *mSphere*, 4, <https://doi.org/10.1128/mSphere.00626-18>, 2019.

505 George, G. D.: The impact of the North Atlantic Oscillation on the development of ice on Lake Windermere, *Climatic
506 Change* 81, 455–468, <https://doi.org/10.1007/s10584-006-9115-5>, 2007.

507 Griffiths, K., Michelutti, N., Sugar, M., Douglas, M. S. V., and Smol, J. P.: Ice-cover is the principal driver of ecological
508 change in high Arctic lakes and ponds, *PLoS One*, 12, <https://doi.org/10.1371/journal.pone.0172989>, 2017.

509 Hampton, S. E., and Galloway, A. W. E., et al.: Ecology under lake ice, *Ecol. Lett.*, 20, 98–111,
510 <https://doi.org/10.1111/ele.12699>, 2017.

511 Iliescu, D., and Baker, I.: The structure and mechanical properties of river and lake ice, *Cold Reg. Sci. Tech.*, 48, 202–217,
512 <https://doi.org/10.1016/j.coldregions.2006.11.002>, 2007.

513 Jakkila, J., Leppäranta, M., Kawamura, T., Shirasawa, K., and Salonen K.: Radiation transfer and heat budget during the
514 melting season in Lake Pääjärvi, *Aquat. Ecol.*, 43, 681–692, <https://doi.org/10.1007/s10452-009-9275-2>, 2009.

515 Karetnikov, S., Leppäranta, M., and Montonen, A.: Time series over 100 years of the ice season in Lake Ladoga, *J. Gt.
516 Lakes Res.*, 43, 979–988, <https://doi.org/10.1016/j.jglr.2017.08.010>, 2017.

517 Kirillin, G., Leppäranta, M., Terzhevik, A., Granin, N., Bernhardt, J., Engelhardt, C., Efremova, T., Golosov, S., Palshin, N.,
518 Sherstyankin, P., Zdorovennova, G., and Zdorovennov, R.: Physics of seasonally ice-covered lakes: a review, *Aquat.
519 Sci.*, 74, 659–682, <https://doi.org/10.1007/s00027-012-0279-y>, 2012.

520 Kirillin, G., Aslamov, I., Leppäranta, M., and Lindgren, E.: Turbulent mixing and heat fluxes under lake ice: the role of
521 seiche oscillations, *Hydrol. Earth Syst. Sci.*, 22, 6493–6504, <https://doi.org/10.5194/hess-22-6493-2018>, 2018.

522 Korhonen, J.: Long-term changes in lake ice cover in Finland, *Hydrol. Res.*, 37, 347–363,
523 <https://doi.org/10.2166/nh.2006.019>, 2006.

524 Langway, C. C.: Ice fabrics and the universal stage, Department of Defense, Department of the Army, Corps of Engineers,
525 Snow Ice and Permafrost Research Establishment, 1959.

526 Lei, R., Leppäranta, M., Erm, A., Jaatinen, E., and Pärn, O.: Field investigations of apparent optical properties of ice cover in
527 Finnish and Estonian lakes in winter 2009, *Est. J. Earth Sci.*, 60, 50–64, <https://doi.org/10.3176/earth.2011.1.05>, 2011.

528 Leppäranta, M.: Interpretation of statistics of lake ice time series for climate variability, *Hydrol. Res.*, 45, 673–683,
529 <https://doi.org/10.2166/nh.2013.246>, 2014.

530 Leppäranta, M.: Freezing of lakes and the evolution of their ice cover, Springer, Berlin-Heidelberg,
531 <https://doi.org/10.1007/978-3-642-29081-7>, 2015.

532 Leppäranta, M., and Kosloff, P.: The thickness and structure of Lake Pääjärvi ice, *Geophysica*, 36, 233–248, 2000.

533 Leppäranta, M., and Wen, L. J.: Ice phenology in Eurasian lakes over spatial location and altitude, *Water*, 14,
534 <https://doi.org/10.3390/w14071037>, 2022.

535 Leppäranta, M., Tikkainen, M., and Virkanen J.: Observations of ice impurities in some Finnish lakes, *Proc. Estonian Acad.
536 Sci. Chem.*, 52, 59–75, 2003.

537 Leppäranta, M., Terzhevik, A., and Shirasawa, K.: Solar radiation and ice melting in Lake Vendyurskoe, Russian Karelia,
538 *Hydrol. Res.*, 41, 50-62, <https://doi.org/10.2166/nh.2010.122>, 2010.

539 Leppäranta, M., Lindgren, E., Wen, L. J., and Kirillin, G.: Ice cover decay and heat balance in Lake Kilpisjärvi in Arctic
540 tundra, *J. Limnol.*, 78, 163–175, <https://doi.org/10.4081/jlimnol.2019.1879>, 2019.

541 Li, Z. J., Jia, Q., Zhang, B. S., Leppäranta, M., Lu, P., Huang, W. F.: Influences of gas bubble and ice density on ice
542 thickness measurement by GPR, *Appl. Geophys.*, 7, 105–113, <https://doi.org/10.1007/s11770-010-0234-4>, 2010.

543 Magnuson, J., Robertson, D., Benson, B., Wynne, R., Livingstone, D., Arai, T., Assel, R., Barry, R., Card, V., Kuusisto, E.,
544 Granin, N., Prowse, T., Stewart, K., and Vuglinski, V.: Historical trends in lake and river ice cover in the Northern
545 Hemisphere, *Science*, 289, 1743–1746, <https://doi.org/10.1126/science.289.5485.1743>, 2000.

546 Masterson D. M.: State of the art of ice bearing capacity and ice construction, *Cold Reg. Sci. Tech.*, 58, 99-112,
547 <https://doi.org/10.1016/j.coldregions.2009.04.002>, 2009.

548 Rouse, W. R., Binyamin, J., Blanken, P. D., Bussières, N., Duguay C. R., Oswald, C. J., Schertzer, W. M., and Spence, C.:
549 The influence of lakes on the regional energy and water balance of the central Mackenzie River Basin, In: *Cold Region
550 Atmospheric and Hydrologic Studies: The Mackenzie GEWEX Experience*, edited by Woo, M. K., Springer, Berlin,
551 309–325, 2008a.

552 Rouse, W. R., Blanken, P. D., Duguay, C. R., Oswald, C. J. and Schertzer, W. M. : Climate-lake interactions. In: *Cold
553 Region Atmospheric and Hydrologic Studies: The Mackenzie GEWEX Experience*, edited by Woo, M. K., Springer,
554 Berlin, 139–160, 2008b.

555 Schroth, A. W., Giles, C. D., Isles, P. D. F., Xu, Y. Y., Perzan, Z., and Druschel, G. K.: Dynamic coupling of iron,
556 manganese, and phosphorus behavior in water and sediment of shallow ice-covered eutrophic lakes, *Environ. Sci.
557 Technol.*, 49, 9758–9767, <https://doi.org/10.1021/acs.est.5b02057>, 2015.

558 SFS 3008: Determination of total residue and total fixed residue in water, sludge and sediment, Finnish Standards
559 Association (SFS), 1990.

560 SFS-EN 27888: Water quality. Determination of electrical conductivity, Finnish Standards Association (SFS), 1994.

561 Sharma, S., Blagrave, K., Magnuson, J. J., O'Reilly, C. M., Oliver, S.; Batt, R. D., Magee, M. R., Straile, D., Weyhenmeyer,
562 G. A., and Winslow, L.: Widespread loss of lake ice around the Northern Hemisphere in a warming world, *Nat. Clim.
563 Chang.*, 9, 227–231, <https://doi.org/10.1038/s41558-018-0393-5>, 2019.

564 Shirasawa, K., Leppäranta, M., Kawamura, T., Ishikawa, M., and Takatsuka, T.: Measurements and modelling of the
565 water-ice heat flux in natural waters, *Proceedings of the 18th IAHR International Symposium on Ice*, Hokkaido
566 University, Sapporo, Japan, 28 August–September 2006, 85–91, 2006.

567 Shoshany, Y., Prialnik, D., Podolak, M.: Monte Carlo modeling of the thermal conductivity of porous cometary ice. *Icarus*,
568 157, 219–227, <https://doi.org/10.1006/icar.2002.6815>, 2002.

569 Stefan, H. G., and Fang, X.: Simulated climate change effects on ice and snow covers on lakes in a temperate region, *Cold
570 Reg. Sci. Tech.*, 25, 137–152, [https://doi.org/10.1016/S0165-232X\(96\)00023-7](https://doi.org/10.1016/S0165-232X(96)00023-7), 1997.

571 Tan, Z., Yao, H. X., and Zhuang, Q. L.: A small temperate lake in the 21st century: Dynamics of water temperature, ice
572 phenology, dissolved oxygen, and chlorophyll a, *Water Resour. Res.*, 54, 4681–4699,
573 <https://doi.org/10.1029/2017WR022334>, 2018.

574 Vehmaa, A., and Salonen, K.: Development of phytoplankton in Lake Pääjärvi (Finland) during under-ice convective mixing
575 period, *Aquat. Ecol.*, 43, 693–705, <https://doi.org/10.1007/s10452-009-9273-4>, 2009.

576 Wang, C. X., Shirasawa, K., Leppäranta, M., Ishikawa, M., Huttunen, O., and Takatsuka T.: Solar radiation and ice heat
577 budget during winter 2002–2003 in Lake Pääjärvi, Finland, *Verh. Internat. Verein Limnol.*, 29, 414–417,
578 <https://doi.org/10.1080/03680770.2005.11902045>, 2005.

579 Warren, S. G.: Optical properties of snow, *Rev. Geophys.*, 20, 67–89, <https://doi.org/10.1029/RG020i001p00067>, 1982.

580 Williams, G., Layman, K. L. and Stefan, H. G.: Dependence of lake ice covers on climatic, geographic and bathymetric
581 variables, *Cold Reg. Sci. Tech.*, 40, 145–164, <https://doi.org/10.1016/j.coldregions.2004.06.010>, 2004.

582 Yang, Y., Leppäranta, M., Cheng, B., and Li, Z. J.: Numerical modelling of snow and ice thicknesses in Lake Vanajavesi,
583 Finland, *Tellus Ser. A, Dyn. Meteorol. Oceanogr.*, 64, <https://doi.org/10.3402/tellusa.v64i0.17202>, 2012.